Photoluminescence properties of Ce^{3+} and Mn^{2+}-activated $Ba_9Sc_2Si_6O_{24}$ phosphor for white light emitting diodes*

Bian Liu(边 柳), Wang Ting(王 婷), Song Zhen(宋 振),
Liu Zhao-Hui(刘朝晖), Li Jia-Xu(李嘉旭), and Liu Quan-Lin(刘泉林)†

School of Materials Science & Engineering and State Key Laboratory for Advanced Metals and Materials, University of Science and Technology Beijing, Beijing 100083, *China*

(Received 26 January 2013; revised manuscript received 4 March 2013)

A single-phased silicate compound $(Ba_{1-x}Ce_x)_{9(}Sc_{1-y}Mn_y)_2Si_6O_{24}$ was prepared by solid-state reaction at high temperature. From powder X-ray diffraction (XRD) analysis, the formation of $Ba_9Sc_2Si_6O_{24}$ with an *R*3 space group was confirmed. In the photoluminescence spectra under ultraviolet (UV) ray excitation, the $Ba_9Sc_2Si_6O_{24}$:Ce^{3+}, Mn^{2+} phosphor emits two distinctive color light bands: a blue one originating from Ce^{3+} and a red one caused by Mn^{2+}. The energy transfer process from Ce^{3+} to Mn^{2+} was confirmed, the critical radius as well as the transfer efficiency was calculated, and the energy transfer mechanism was discussed. In addition, the decay-time testing indicates that the energy transfer efficiencies from Ce(1) to Mn^{2+} and Ce(2) to Mn^{2+} are different. The emission chromaticity of $Ba_9Sc_2Si_6O_{24}$:Ce^{3+}, Mn^{2+} phosphor could be tuned from blue to red by altering the Ce^{3+}/Mn^{2+} concentration ratio.

Keywords: $Ba_9Sc_2Si_6O_{24}$, Ce^{3+}, Mn^{2+} co-doped, energy transfer

PACS: 78.55.–m, 87.15.mq, 33.50.–j **DOI:** 10.1088/1674-1056/22/7/077801

1. Introduction

In recent years, white light-emitting diodes (WLEDs) have been a hot topic due to their advantages of low energy consumption, long lifetime, and no pollution as well as their potential applications in lighting fields.[1,2] The most common way to obtain WLEDs is the combination of blue LED chips with yellow light emitting phosphors YAG:Ce^{3+}, which was introduced by Nichia in 1996.[3] However, this kind of WLED has the following problems: changing color with the input power, low color rendering index (CRI), and low reproducibility.[4,5] To solve these problems, the WLED has been fabricated by employing blue, green, and red emitting multiphase phosphors excited by an ultraviolet (UV) chip.[6] In this system, the performances of white LEDs, including the CRI, color temperature, and color range, can be significantly dependent on the employed phosphors.[7] Therefore, novel UV excitation phosphors with improved properties are greatly in demand.

Among these phosphors, Mn^{2+}-activated phosphor becomes a new candidate for red-emitting materials, and is considered as an excellent phosphor material for WLED applications. In Mn^{2+} ions, the absorption transitions to the excited state are spin-forbidden with low transition probabilities, and the emission intensity from Mn^{2+} ions, excited by UV, would be intrinsically weak. However, Mn^{2+} co-doped with Ce^{3+} can create efficient red-band emission with the help of energy transfer from Ce^{3+}, which can absorb near UV light well. Ce^{3+}/Mn^{2+} co-doped silicates,[8] borates,[9] aluminates,[10] and phosphates[11] have become hot topics in recent years. Especially, Ce^{3+} and Mn^{2+} co-doped alkaline earth silicate was found to be a promising candidate host, which has a stable crystal structure and can be easily produced.[12]

$Ba_9Sc_2Si_6O_{24}$(BSSO), as a new silicate candidate for the phosphor matrix, was first synthesized and initially characterized by Wang *et al.*[13] in 1994. In recent years, research on its stable crystal structure and good luminescent properties when doped with Eu^{2+} were reported.[14,15] However, there is no report on BSSO co-doped with Ce^{3+} and Mn^{2+}. In view of the effective ionic radii of cations with different coordination numbers, it is predicted that Ce^{3+} ($^{XII}r^{3+}$ = 1.34 Å, 1 Å = 0.1 nm) and Mn^{2+} ($^{VI}r^{2+}$ = 0.81 Å) prefer to occupy the Ba^{2+} ($^{XII}r^{2+}$ = 1.61 Å) and Sc^{3+}($^{VI}r^{3+}$ = 0.85 Å) sites, respectively. In this study, $Ba_9Sc_2Si_6O_{24}$:Ce^{3+}, Mn^{2+} (BSSO:Ce^{3+}, Mn^{2+}) phosphors emitting blue and red lights with the variations in the content of Ce^{3+} and Mn^{2+} are synthesized. According to our previous work, BSSO:Ce^{3+} emits blue light and the emission peak positions change gradually with the increase of the content of Ce^{3+}, owing to the presence of two types luminescence centers of Ce^{3+}.[16] Hence, we designed and synthesized two groups of samples, i.e., BSSO:0.045Ce^{3+}, *y*Mn^{2+} and BSSO:0.27Ce^{3+}, *y*Mn^{2+}, to investigate their luminescent properties. The two groups of samples were examined by X-ray diffraction (XRD), steady state spectra, and transient state spectra. We then reported efficient energy transfer from the Ce^{3+} ion to the Mn^{2+} ion, the critical

*Project supported by the National Natural Science Foundation of China (Grant No. 51272027) and the Specialized Research Fund for the Doctoral Program of Higher Education of China (Grant No. 20100006110011).

†Corresponding author. E-mail: qlliu@ustb.edu.cn

© 2013 Chinese Physical Society and IOP Publishing Ltd

radius, and the resonance energy type, and the distinguished two types of sensitizer Ce^{3+} ions for Mn^{2+} ions. The emission chromaticity of $Ba_9Sc_2Si_6O_{24}$:Ce^{3+}, Mn^{2+} phosphor could be tuned from blue to red by altering the Ce^{3+}/Mn^{2+} concentration ratio.

2. Experiment

Samples with the general composition $(Ba_{1-x}Ce_x)_9(Sc_{1-y}Mn_y)_2Si_6O_{24}$ were prepared by solid-state reactions and were divided into two groups by the concentration of Ce: group A with low concentration of Ce, i.e., $x = 0.045$ and $y = 0$, 0.015, 0.03, 0.045, 0.09, 0135, 0.18, 0.36, and 0.45, and group B with high concentration of Ce, $x = 0.27$ and $y = 0$, 0.09 0.18, 0.27, 0.36, 0.45, 0.54, and 0.63. The starting reagents were $BaCO_3$ (analytical reagent (A.R.)), Sc_2O_3(A.R.), SiO_2 (A.R.), CeO_2(99.9%), and MnO_2(A.R.). The raw materials were weighted stoichiometrically and mixed thoroughly in an agate mortar, then were calcined in a 10% H_2–90% N_2 atmosphere at 1350 °C for 3 h.

XRD patterns of the products were recorded on a Philips X'Pert PW-3040 diffract meter (45 kV×40 mA) with Cu Kα1 radiation ($\lambda = 0.15406$ nm). Continuous scan mode with a 2θ scan range of 10°–80° was employed. These XRD data were analyzed by the Rietveld refinement program FullProf.2k based on the structure model of $Ba_9Sc_2Si_6O_{24}$ reported by Wang *et al.*[13] The photoluminescence (PL) and photoluminescence excitation (PLE) spectra were measured with an Edinburgh Instruments FLS920 spectrofluorimeter equipped with a continuous 450-W Xenon lamp. For low temperature measurements, the samples were mounted on a closed cycle cryostat (10 K–450 K, DE202, Advanced Research Systems). Slit widths of 0.3 nm were used on the excitation and emission monochromators. The step width was 1.0 nm and the dwell time was 0.20 s. The line intensities and positions of the measured spectra were corrected by the FLS920 correction curve.

3. Results and discussion

The silicate compound $Ba_9Sc_2Si_6O_{24}$ was reported to crystallize in a rhombohedra structure with the space group $R3$ (No. 148), having unit cell dimensions close to $a = 9.8716(2)$ Å, $c = 21.9376(7)$ Å.[13] Ba^{2+} ions were divided into two types according to their coordination: Type I is Ba(1) with 12-fold coordination number (CN = 12) and the average bond-length around Ba(1) is 3.047 Å. Type II includes Ba(2) (CN = 9) and Ba(3) (CN = 10) and their average bond-lengths are 2.899 Å and 2.903 Å, respectively, which is much shorter versus type I. Sc^{3+}occupies one crystallographic site with six-fold coordination. The schematic crystal structure model of $Ba_9Sc_2Si_6O_{24}$ viewed along the c axis, b axis and the coordination of the Ba^{2+} are shown in Fig. 1. In view of the effective ionic radii of cations with different coordination numbers, it is predicted that Ce^{3+} and Mn^{2+} prefer to occupy the Ba^{2+} and Sc^{3+} sites, respectively. The valence would be balanced owing to the vacancy of O^{2-} ions.

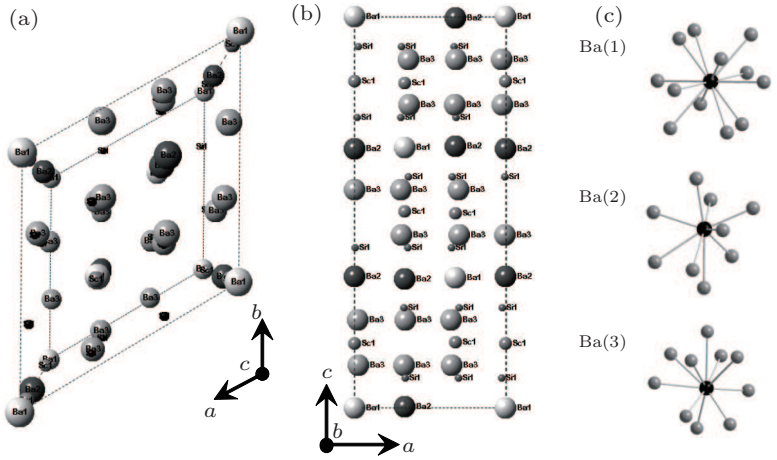


Fig. 1. Schematic crystal structure model of $Ba_9Sc_2Si_6O_{24}$ viewed along the (a) c axis, (b) b axis, and (c) the coordination of Ba^{2+}, respectively.

Figure 2 shows two typical X-ray diffraction patterns (XRD) of $Ba_9Sc_2Si_6O_{24}$:0.045Ce^{3+}, 0.09Mn^{2+} (Fig. 2(a)) belonging to group A, and $Ba_9Sc_2Si_6O_{24}$:0.27Ce^{3+}, 0.63Mn^{2+} (Fig. 2(b)) belonging to group B. All diffraction peaks match well with the $Ba_9Sc_2Si_6O_{24}$ phase (Fig. 2(c)) from JCPDS file No. 82-1119). All XRD patterns of the samples (not shown here) signify that, in the dopant concentration ranges investigated in this study, the incorporation of Ce^{3+} and Mn^{2+} ions into the $Ba_9Sc_2Si_6O_{24}$ lattice does not produce any significant change to the crystal structure of the host matrix. However, with the increase of the doping concentration of Ce^{3+} and Mn^{2+}, the lattice pentameters were changed. As shown in Fig. 3, the lattice parameters a and c of BSSO:Ce^{3+}, Mn^{2+} from groups A and B decrease with the increase of Ce^{3+} and

Mn^{2+} concentration, which is reasonable because the radii of Ce^{3+} and Mn^{2+} are smaller than those of Ba^{2+} and Sc^{3+}, respectively. The decreasing relations confirm that Ce^{3+} and Mn^{2+} ions have substituted Ba^{2+} and Sc^{3+} ions successfully in the lattice.

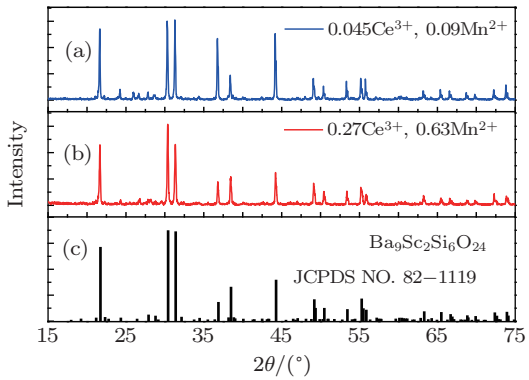


Fig. 2. (color online) (a) XRD patterns of the BSSO:0.045Ce^{3+}, 0.09Mn^{2+} powder, (b) BSSO:0.27Ce^{3+}, 0.63Mn^{2+} powder, and (c) JCPDS of BSSO.

According to our previous work,[16] we find that at room temperature under UV light excitation, the phosphors BSSO:Ce^{3+}emit blue light and the emission peak shifts from 382 nm to 405 nm with the increase of Ce^{3+} concentration. These phenomena could be explained by the two types of Ce^{3+}luminescence centers in the BSSO:Ce^{3+}. Herein, to study the sensitive properties between low/high concentration of Ce^{3+} and Mn^{2+}, we have synthesized two groups of samples: group A (BSSO:0.045Ce^{3+}, $y$$Mn^{2+}$) and group B (BSSO:0.27$Ce^{3+}$, $y$$Mn^{2+}$) as described above.

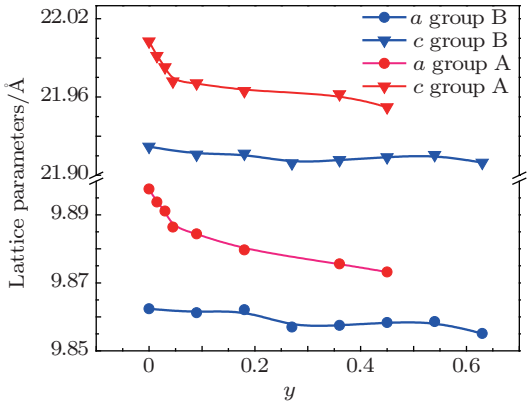


Fig. 3. (color online) The lattice parameters of a and c of group A (BSSO:0.045Ce^{3+}, $y$$Mn^{2+}$ (y = 0–0.45)) (red) and group B (BSSO:0.27Ce^{3+}, $y$$Mn^{2+}$ (y = 0–0.63)) (blue).

It is known that tetrahedral coordinated Mn^{2+} ions (weak crystal-field) usually give a green emission and octahedral coordinated Mn^{2+} ions (strong crystal-field) give an orange to red emission.[8] However, the d–d absorption transition of Mn^{2+} ion is strongly forbidden, and thus its excitation efficiency is very low in many silicate phosphors. We prepared BSSO:Mn^{2+} samples only doped with different concentrations of Mn^{2+} and could not detect their luminescence. However, when BSSO:Mn^{2+} was doped with the second doped ions, Ce^{3+}, even though in a small amount, we found powerful luminescence. The same phenomena were reported in $Ba_3MgSi_2O_8$:Eu^{2+}, Mn^{2+}[17] compound.

Figures 4 and 5 show the PLE (insets) and PL spectra of group A (BSSO:0.045Ce^{3+}, $y$$Mn^{2+}$) and group B (BSSO:0.27$Ce^{3+}$, $y$$Mn^{2+}$), respectively. All the emission spectra were measured under 328-nm excitation, and thus their luminescence were comparable. As shown in Figs. 4 and 5, the short wavelength bands peaking at around 400 nm were from Ce^{3+} and the long wavelength bands peaking at 621 nm were from Mn^{2+}. With the doping Mn^{2+} concentration increasing, the emission intensity of Ce^{3+} weakens, while the emission intensity of the Mn^{2+} ions increases systematically till their saturation points. The dependence of the emission intensity on Mn^{2+} concentration also supports the energy transfer between Ce^{3+} and Mn^{2+} ions. The excitation spectra of Ce^{3+} and Mn^{2+} were accordingly shown in the insets of Figs. 4 and 5. The excitation spectra monitoring the Mn^{2+} -derived emission are overlapped with the excitation bands of Ce^{3+}, which implies that a part of the energy absorbed by Ce^{3+} ions could be transferred to Mn^{2+} ions.

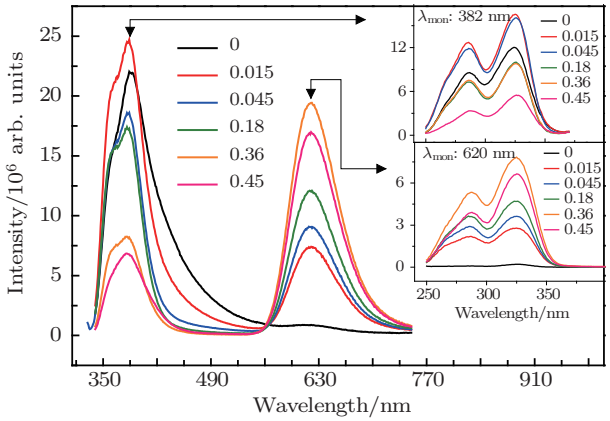


Fig. 4. (color online) PL of BSSO: 0.045Ce^{3+}, $y$$Mn^{2+}$ and insets are their two PLE (different line colors represent different concentrations of Mn^{2+}).

Comparing the emission spectra of groups A and B in detail, we find that the emission peak of Ce^{3+} locates at $\sim$ 382 nm for the samples with high concentration (group A), while at $\sim$ 405 nm for the samples in group B, which is owing to the various concentration of Ce^{3+} In addition, the quenching concentration of Mn^{2+} for the samples in group A is about 0.36, while about 0.45 for the samples in group B. There exists a difference between PLES of Ce^{3+} in groups A and B. The PLE spectrum monitoring Mn^{2+} is almost the same as that monitoring Ce^{3+} for the samples in group A (the insets of Fig. 4), while the PLE spectrum of Mn^{2+} is obviously different from that of Ce^{3+} for the samples in group B (the insets of Fig. 5). These phenomena indicate that Ce^{3+} ions in the samples of group A are easier to transfer their energy to Mn^{2+} ions comparing with those in group B.

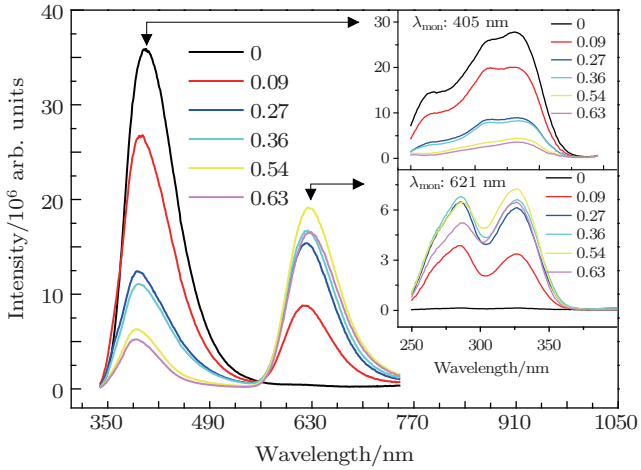


Fig. 5. (color online) PL and PLE of BSSO:0.27Ce^{3+}, yMn^{2+} and insets are their two PLE (different line colors represent different concentrations of Mn^{2+}).

Figure 6 shows the integrated emission intensity of Ce^{3+}, Mn^{2+}, and the total from group A and group B, respectively. In the group A (Fig. 6(a)), with the concentration of Mn^{2+} increasing, the total intensity does not change greatly. However, in group B (Fig. 6(b)), the total integrated intensity gradually decreases with Mn^{2+} concentration increasing. This phenomenon could be explained by considering that the energy transfer between Ce^{3+} and Mn^{2+} increases the possibility of non-radiative transition due to the dissimilarity of their excitation spectra in group B.

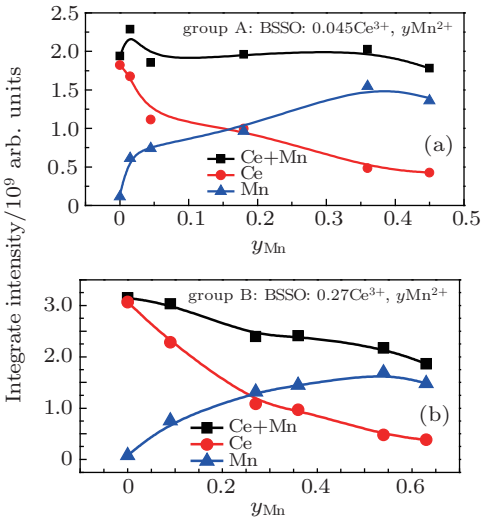


Fig. 6. (color online) The integrated intensity of BSSO:Ce^{3+}, Mn^{2+} in groups A (a) and B (b) versus Mn concentrations. The red line with trigons represents the emission intensity of Ce, the blue line with circles represents the emission intensity of Mn^{2+}, and the black line with diamonds represents the total emission intensity of Ce^{3+} and Mn^{2+}.

While considering the mechanism of energy transfer in oxide phosphors, Blasse[18] has pointed out that if the activator was introduced solely on Z-ion sites, the critical transfer distance R_c is approximately equal to twice the radius of a sphere within this volume

$$R_c = 2\left(\frac{3V}{4\pi X_c N}\right)^{1/3},$$

where X_c is the critical concentration (molar percentage), N is the number of Z ions in the unit cell, and V is the volume of the unit cell. For the two different activators doped in two different sites, X_cN should be the weighted average of Ce^{3+} and Mn^{2+} which were doped in Ba and Sc sites, respectively. The equation was changed to

$$R_{Ce,Mn} = 2\left[\frac{3V}{4\pi(X_{Ce}N_{Ce} + X_{Mn}N_{Mn})}\right]^{1/3}.$$

For the BSSO:Ce^{3+}, Mn^{2+} host lattice, $V = 1851.38$ Å^3, $N_{Ce} = 27$, and $N_{Mn} = 6$. The critical concentrations X_{Ce} and X_{Mn} are defined as the value at which the luminescence intensity of Ce^{3+} reduces to half of that for the sample in the absence or presence of Mn^{2+}.[19–21] Here, we take $X_{Ce} = 0.5\%$ and $X_{Mn} = 9.0\%$ for group A, and $X_{Ce} = 3.0\%$ and $X_{Mn} = 10.5\%$ for group B, the $R_{Ce,Mn}$ of groups A and B are calculated to be 17.4 Å and 13.5 Å, respectively.

The energy transfer efficiency η_T from Ce^{3+} to Mn^{2+}has been discussed by Paulose *et al.*[22] and can be calculated by the following formula:

$$\eta_T = \frac{I_{S0} - I_S}{I_{S0}},$$

where I_S and I_{S0} are the luminescence intensities of the sensitizer (Ce^{3+}) with and without an activator (Mn^{2+}), respectively. Figure 7 shows the results of energy transfer efficiency from Ce^{3+} to Mn^{2+} for groups A and B, respectively. The energy transfer efficiency increases with the increase of the Mn^{2+} concentration, and we find that no matter whether the doping concentration of Ce^{3+} is high or low, the ET efficiency lines are nearly coincident. This means that η_T is more related to the amount of activators rather than that of sensitizers.

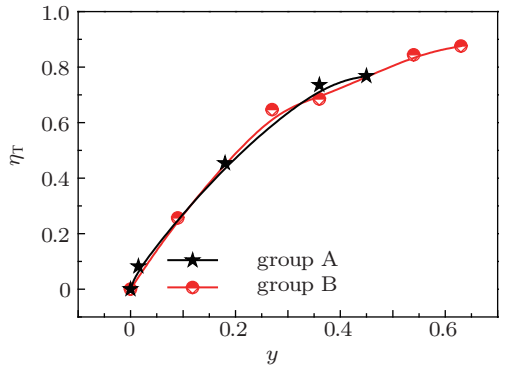


Fig. 7. (color online) Energy transfer efficiencies η_T of group A and group B versus Mn concentration y.

The energy transfer mechanism between Ce^{3+} and Mn^{2+} in BSSO:Ce^{3+}, Mn^{2+} should be controlled by an electric multipole–multipole interaction according to Dexter's theory and Reisfeld's approximation. The energy transfer can be described by the following equation:[23,24]

$$\frac{I_{S0}}{I_S} \propto C^{n/3},$$

where I_{S0} is the intrinsic luminescence intensity of Ce^{3+}, I_S is the luminescence intensity of Ce^{3+} in the presence of the Mn^{2+}, C is the concentration of Mn^{2+}; $n = 6$, 8, and 10, representing the dipole–dipole, dipole–quadrupole, and quadrupole–quadrupole interactions, respectively. The value of n can be determined from the slope (n/3) of the linear line. Figures 8(a)–8(c) and figures 8(d)–8(f) show the plots of $I_{S0}/I_S - C^{n/3}$ for groups A and B, respectively. The results indicate that a linear behavior was observed only when $n = 6$, in both of groups A and B. So that the energy absorbed by Ce^{3+} is transferred to Mn^{2+} by a nonradiative dipole–dipole interaction. This indicates that the dipole–dipole interaction is the energy transfer mechanism between Ce^{3+} and Mn^{2+} in the BSSO:Ce^{3+}, Mn^{2+} phosphor.

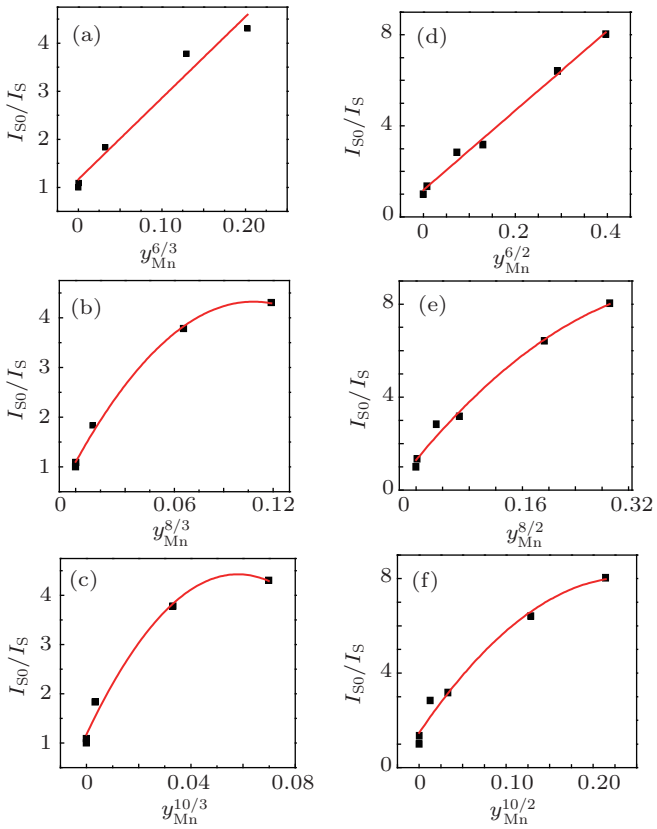


Fig. 8. (color online) The dependence of I_{S0}/I_S of Ce^{3+} on (a) $C^{6/3}$, (b) $C^{8/3}$, and (c) $C^{10/3}$ based on group A, respectively. The dependence of I_{S0}/I_S of Ce^{3+} on (d) $C^{6/3}$, (e) $C^{8/3}$, and (f) $C^{10/3}$ based on group B, respectively.

Our previous work showed that the emission peak positions of BSSO:Ce^{3+}change gradually with the increase of the content of Ce^{3+}, owing to the presence of two types of Ce^{3+}luminescence centers of Ce^{3+},[16] i.e., Ce(1) peaking at 382 nm and Ce(2) peaking at 420 nm. When the concentration was low, Ce(1) plays a dominant role, while Ce(2) is dominant at high concentration owing to the energy transfer from Ce(1) to Ce(2). Hence, we measured the fluorescence lifetimes of 382 nm (Ce(1)), 420 nm (Ce(2)) emissions in BSSO:0.27Ce^{3+}, yMn^{2+} ($y = 0$, 0.09, 0.18, 0.27, 0.36, 0.45, 0.54, and 0.63). All the decay curves could be fitted by a single exponential function, and their lifetimes are presented in the Figs. 9(a) and 9(b). Some representative sample decay curves ($x = 0$, 0.09, 0.27, and 0.54) are shown in the insets of the Figs. 9(a) and 9(b). The reduction of the lifetimes for Ce^{3+} at different luminescence centers with Mn^{2+} concentration increasing are observed, which are strong evidence for the energy transfer from Ce^{3+} to Mn^{2+} ions. Without Mn^{2+} ions doping, the lifetime of Ce(1) is about 20 ns, which is shorter than that of Ce(2), i.e., $\sim$ 30 ns. According to the theory, the sensitizer with a short lifetime will transfer energy easily.[25] We predict that Ce(1) transfers energy to Mn^{2+} more efficiently than Ce(2). The results are supported by the PLE spectra shown in the insets of Figs. 4 and 5. The PLE spectra of Mn^{2+} and Ce^{3+} are very similar to each other in group A. This suggests the energy transfers mainly occur between Ce(1) and Mn^{2+} at low Ce^{3+} concentration (Fig. 4). However, a large difference between the PLE of Mn^{2+} and Ce^{3+} in group B (Fig. 5) may indicate that Ce(1) can transfer energy to Mn^{2+} more efficiently than Ce(2).

To better understand the difference in the energy transfer of Ce(1) and Ce(2) to Mn^{2+}, we calculate their energy transfer efficiency (η_τ) by

$$\eta_\tau = 1 - \frac{I_S}{I_{S0}},$$

where τ_{S0} is the decay time of Ce^{3+} in the absence of Mn^{2+}, and τ_S is the decay time of Ce^{3+} in the presence of Mn^{2+}. The results of $\eta_{\tau 1}$ for Ce(1) and $\eta_{\tau 2}$ for Ce(2) are shown in Table 1. The $\eta_{\tau 1}$ and $\eta_{\tau 2}$ are both increased with the increase of content of Mn^{2+}, which also demonstrates the occurrence of the energy transfer from Ce(1) and Ce(2) to Mn^{2+}. However, $\eta_{\tau 1}$ is always higher than $\eta_{\tau 2}$, indicating that Ce(1) transfers energy to Mn^{2+} more efficiently than Ce(2).

The lifetime of the Mn^{2+}ions in group A is the same as that of group B, i.e., $\sim$ 2.3 ms. This long lifetime is a typical characteristic of the parity and spin forbidden $^4T_g(^4G)$–$^6A_g(^6S)$ transition of Mn^{2+}. We give the variations of the lifetimes of Mn^{2+} in group B with increasing Mn^{2+} concentration in Fig. 9(c). It has been reported that an increase of Mn^{2+} concentration produces a decrease of Mn^{2+} luminescence lifetime. This can be explained in terms of the cross-relaxation interactions between the close Mn^{2+} pairs.

Table 1. ET efficiencies of Ce(1) to Mn^{2+} and Ce(2) to Mn^{2+}.

yMn	0.09	0.18	0.27	0.36	0.45	0.54	0.63
Ce(1)/$\eta_{\tau 1}$	12.28%	35.03%	36.63%	36.63%	40.69%	42.17%	38.30%
Ce(2)/$\eta_{\tau 2}$	5.71%	28.93%	28.43%	28.79%	30.95%	34.55%	30.00%

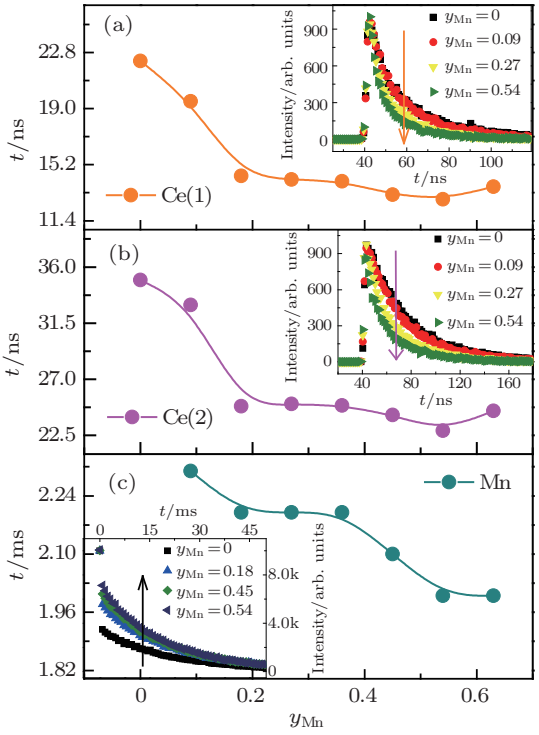


Fig. 9. (color online) The decay time of (a) Ce(1), (b) Ce(2), and (c) Mn of BSSO:0.27Ce^{3+}, yMn^{2+} ($y = 0$–0.63). Insets are the decay curves of some representative samples.

It is worth noting that the as-obtained BSSO:Ce^{3+}, Mn^{2+} sample can give multicolor emissions (blue and red). We find that the relative intensities of the two color parts can be tuned by varying concentrations of Ce^{3+} and Mn^{2+}. Figure 10 shows the CIE chromaticity coordinates of the samples from group A (black circles) and group B (white circles) measured under the excitation of 328 nm with different Mn^{2+} concentrations. It is clearly observed that the CIE chromaticity coordinates shift from the blue region to the red region with the increase of Mn^{2+} content from 0 mol% to 27.0 mol%. In addition, if mixing the BSSO:0.045Ce, 0.045Mn with some green phosphors

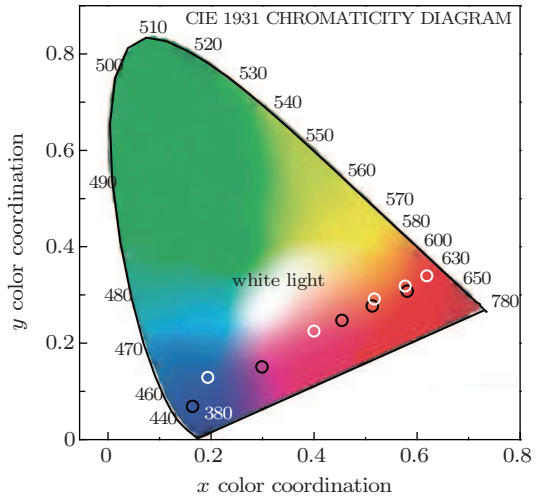


Fig. 10. (color online) CIE 1931 chromaticity coordinates diagrams of BSSO: 0.045Ce^{3+}, yMn^{2+} (black circles), and BSSO:0.27Ce^{3+}, yMn^{2+} (white circles).

i.e., BSSO:Eu^{2+}, and coating on an NUV-chip, we can get a pure white light emitting diode.

4. Conclusions

Two groups of single-host phosphors $(Ba_{1-x}Ce_x)_9(Sc_{1-y}Mn_y)_2Si_6O_{24}$ were prepared by the high-temperature solid-state reaction. The phosphors exhibit strong blue and red emissions under the UV excitation. A bright red emission from Mn^{2+} is obtained only if Ce^{3+} ions are co-doped together. The energy transfer process from Ce^{3+} to Mn^{2+} in a BSSO matrix has been demonstrated via diploe–diploe mechanism. The critical radii with low and high concentrations of Ce^{3+} are calculated to be 17.4 Å and 13.5Å, respectively. The lifetime of luminescence center Ce(1) is shorter than that of Ce(2), and the PLE spectra of Ce(1) is coincident with that of Mn^{2+}, confirming that luminescence centers Ce(1) can transfer energy to Mn^{2+} more efficiently than Ce(2). The CIE chromaticity coordinates can be tunable from blue to red, which indicates the BSSO:Ce^{3+}, Mn^{2+} may have a potential application in UV-white LEDs.

References

[1] Wei X D, Cai L Y, Lu F C, Chen X L, Chen X Y and Liu Q L 2009 *Chin Phys. B* **18** 3555
[2] Zhou T L, Song Z, Song X P, Bian L and Liu Q L 2010 *Chin. Phys. B* **19** 127808
[3] Nakamura S and Fasol G 1997 *The Blue Laser Diode-GaN Based Light Emitters and Lasers* (Springer: Berlin)
[4] Kuo T W, Liu W R and Chen T M 2010 *Opt. Express* **18** 1888
[5] Huang C H, Chen T M, Liu W R, Chiu Y C, Yeh Y T and Jang S M 2010 *ACS Appl. Mater. Interfaces* **2** 347
[6] Sato Y, Takahashi N and Sato S 1996 *Jpn. J. Appl. Phys. Lett.* **35** L838
[7] Zorenko Y, Gorbenko V, Voznyak T, Batentschuk M, Osvet A and Winnacker A 2010 *J. Lumin.* **130** 380
[8] Li G G, Geng D L, Shang M M, Peng C, Cheng Z Y and Lin J 2011 *J. Mater. Chem.* **21** 13334
[9] Zhang X M, Qiao X B and Seo H J 2011 *Curr. Appl. Phys.* **11** 442
[10] Zhang X G and Gong M L 2007 *J. Lumin.* **127** 483
[11] Zhang J and Wang Y H 2011 *Mater. Chem. Phys.* **130** 1265
[12] Yonesaki Y, Takei T, Kumada N and Kinomura N 2010 *J. Solid State Chem.* **183** 1303
[13] Wang L H, Schneemeyer L F, Cava R J and Siegrist T 1994 *J. Solid State Chem.* **113** 211
[14] Nakano T, Kawakami Y, Uematsu K, Ishigaki T, Tada K and Sato M 2009 *J. Lumin.* **129** 1654
[15] Bian L, Zhou T L, Yang J J, Song Z and Liu Q L 2012 *J. Lumin.* **132** 2541
[16] Bian L, Du F F, Yang S S, Ren Q Y and Liu Q L 2013 *J. Lumin.* **137** 168
[17] Kim J S, Jeon P E and Choi J C, Park H L, Mho S I and Kim G C 2004 *Appl. Phys. Lett.* **84** 2931
[18] Blasse G and Grabmaier B C 1994 *Luminescent Materials* (Berlin: Springer-Verlag) p. 52
[19] Kim Y K, Choi S H and Jung H K 2010 *J. Lumin.* **130** 60
[20] Ju G F, Hu Y H, Chen L and Wang X J 2012 *J. Lumin.* **132** 1792
[21] Ye S, Liu Z S, Wang J G and Jing X P 2008 *Mater. Res. Bull.* **43** 1057
[22] Paulose P I, Jose G, Thomas V, Unnikrishnan N V and Warrier M K R 2003 *J. Phys. Chem. Solids* **64** 841
[23] Dexter D L and Schulman J A 1954 *J. Chem. Phys.* **22** 1063
[24] Reisfeld R, Greengerg E, Velapoldi R and Barnett B 1972 *J. Chem. Phys.* **56** 1698
[25] Sun J Y, Du H Y and Hu W X 2003 *Solid State Luminescent Material* 1st edn. (Beijing: Chemical Industry Press) p. 152